Supporting Information

MXene Nanofibers Confining MnO_x Nanoparticles: A Flexible Anode for High-Speed Lithium Ion Storage Networks

Ying Guo,[a] Deyang Zhang,[a,*] Zuxue Bai,[a] Ya Yang,[a] Yangbo Wang,[a] Jinbing Cheng,[b] Paul K. Chu,[c] and Yongsong Luo[a,b,*]

[a] Key Laboratory of Microelectronics and Energy of Henan Province, School of Physics and Electronic Engineering, Xinyang Normal University, Xinyang 464000, PR China.

[b] Henan International Joint Laboratory of MXene Materials Microstructure, College of Physics and Electronic Engineering, Nanyang Normal University, Nanyang 473061, PR. China.

[c] Department of Physics, Department of Materials Science & Engineering, and Department of Biomedical Engineering, City University of Hong Kong, Tat Chee Avenue, Kowloon, Hong Kong, China.

[*] Corresponding author. Tel./fax: +86 376 6391760, E-mail: ysluo@xynu.edu.cn (Y. S. Luo), zdy@xynu.edu.cn (D. Y. Zhang).

1. Experimental Details

1.1 Materials

Manganese acetate ($C_4H_6MnO_4$, 99%), N, N-dimethyl formamide (DMF, 99.9%), and polyacrylonitrile (PAN, Mw = 150,000) were purchased from Aladdin. All reagents are of analytical grade and used without further purification.

1.2 Synthesis of $Ti_3C_2T_x$ MXene

The Ti_3AlC_2 MAX phase was synthesized by spark plasma sintering system (Model: SPS-211HF) as reported previously.[1] The starting powders (TiC, Ti, and Al powders with molar ratios of 1.8:1.2:1.2) were mixed, ground for 12h, put into a mold with an inner diameter of 15mm, and sintered at 1400 °C for 12 min at a pressure of 30 MPa. The product was ground and sieved through a 400 mesh sieve to produce powders with a particle size less than 35 μm. To accurately etch Al from Ti_3AlC_2, 2 g of Ti_3AlC_2 powders were slowly added to 70 mL of the etching solution containing 60 mL of 9 M HCl, 10 mL of 49% HF, and 1 g LiF. The mixture was maintained at 35 ºC under agitation for 12 h. The multilayer $Ti_3C_2T_x$ MXene was washed repeatedly with deionized water by centrifugation at 5000 rpm until the pH ≥ 6. Next, $Ti_3C_2T_x$ MXene solution was transferred to a special bottle shaking by hand for an hour and then sonicated in the Ar atmosphere for an hour. The solution was washed repeatedly with deionized water by centrifugation at 4000 rpm and the product was collected. To use the product for electrospinning, the solvent (deionized water) was exchanged with dimethylformamide (DMF) by repeated centrifugation (five times) at 10000 rpm and the DMF solution of $Ti_3C_2T_x$ MXene with a concentration of about 40 mg mL^{-1} was obtained.

1.3 Synthesis of MnOx-MXene/CNFs

MnO_x-MXene/CNFs was synthesized by electrospinning and then stepwise annealing. 0.6 g of $C_4H_6MnO_4$ was dispersed in 5mL of Ti_3C_2 solution and stirred for 60 min in an ice bath. 0.5 g of PAN were added and stirred continuously overnight. The electrospinning solution was loaded into a 5 mL plastic syringe equipped with an 18 G blunt-tip needle. A positive voltage (18 kV) was applied to the needle tip and a collector

roller covered with an aluminum foil was grounded. The distance between the needle tip and the collector was 12 cm and the infusion rate of the solution was controlled to be 1.2 mL h^{-1}. The samples were electrospun at a relative humidity below 25%. The electrospun mats were first stabilized in air at 280 ℃ for 1 h at a ramping rate of 5 ℃ min^{-1} and then carbonized under argon at a ramping rate of 2 ℃ min^{-1} at 600 ℃ for up to 3 h.

1.4 Synthesis of MXene/CNFs and MnO_x/CNFs

For comparison, MXene/CNFs and MnO_x/CNFs were prepared. The control sample of MXene/CNFs was prepared in the same way as MnO_x-MXene/CNFs but without addition of $C_4H_6MnO_4$. Similarly, MnO_x/CNFs was prepared without adding $Ti_3C_2T_x$ MXene.

1.5 Materials characterization

The crystalline structure and phase of the composites were identified by X-ray diffraction (XRD, Bruker D2 PHASER) using Cu-Kα (λ=1.5418 Å) radiation at 40 kV and 40 mA, with 2θ between 5° and 80° at room temperature. Raman spectroscopy was carried out using an INVIA Raman microprobe (Renishaw Instruments) with a 532 nm laser source, a 50× objective lens and the laser power is 10%. The chemical elements were analyzed on an X-ray photoelectron spectroscopy (XPS, K-ALPHA 0.5 eV) with a resolution of 0.3-0.5 eV from a monochromated aluminum anode X-ray source. The thermogravimetric (TG) analyzer curve was performed using an STA449F5 (NETZSCH) with 100 mL min^{-1} of oxygen flow from 20 ℃ to 800 ℃ at a heating rate of 10 ℃ min^{-1}. The morphologies were examined on a field emission scanning electron microscope (SEM, Hitachi S-4800), a transmission electron microscope (TEM, Tecnai G2 F20) and an atomic force microscopy (AFM, Bruker Dimension Icon). The elemental analysis was carried out using an energy-dispersive X-ray spectroscope (EDS, Bruker-QUANTAX) attached to the TEM.

1.6 Electrochemical evaluation

The electrochemical measurements were conducted using CR2032-type coin cells assembled in an argon-filled glove box with water and oxygen contents below 0.1 ppm. The as-synthesized MnO_x-MXene/CNFs membrane was cut into free-standing

electrodes with a diameter of 16 mm and a thickness of 0.2 mm (The mass of a single electrode is about 0.0040 g, the area is 2 cm^2, and the mass per unit area is 2 mg cm^{-2}), dried in a vacuum oven at 80°C overnight, and directly assembled into Li-ion batteries. Neither a metal current collector nor any additives (e.g., conductive carbon or binder) was required. In the lithium ion batteries, Li metal was used as the counter and reference electrode and microporous Celgard 2400 membrane was used as the separator. The electrolyte was composed of a solution of 1 mol L^{-1} $LiPF_6$ dissolved in a mixture of ethyl carbonate and dimethyl carbonate (1/1; v/v) with the addition of 5 wt% fluoroethylene carbonate. Cyclic voltammetry (CV) was carried out on a VMP3 electrochemical workstation under different scanning speed. The electrochemical impedance spectroscopy (EIS) was performed by applying a sine wave with an amplitude of 0.5 mV over the frequency range of 0.01 Hz-100 kHz. Galvanostatic charging-discharging tests were performed on a Neware battery testing system in the potential range of 0.01-3.0 V at room temperature. The specific capacity and area capacity are calculated by normalizing the mass loading and area of MnO_x-MXene/CNFs electrode, respectively. MXene/CNFs and MnO_x/CNFs were also made into self-standing electrodes for the same test. Full cell batteries were assembled based on MnO_x-MXene/CNFs anodes and $LiCoO_2$/Al cathodes in coin cell (CR2032) in an Ar-filled glove box. The $LiCoO_2$ cathode was made by slurry containing active powders, conductivity agent (Super-P), and PVDF in a solvent (N-methyl-2-pyrrolidone, NMP) with a mass ratio of 8:1:1. The mass density of $LiCoO_2$ cathode was about 5 mg cm^{-2}. Full cell batteries cycling performance tests were performed on a Neware battery testing system at room temperature.

1.7 Computational details

The experimentally determined lattice parameters of the Mn_3O_4 (a=b=5.763 Å, c=18.3496 Å) and MnO (a=b=4.451 Å, c=18.902 Å) were used in the simulation. The (001) plane was adopted in the simulation models. Here, 2×2 supercells correspond to the lattice of 11.840 Å for Mn_3O_4 and 9.712 Å for MnO along the directions parallel to the surface. Accordingly, a 4×4 supercell of MXene that has a comparable lattice of 12.150 Å was adopted in the simulation. The Mn_3O_4 or MnO (001) surface and a Ti_3C_2

monolayer were bridged by the O atom.

First-principles density functional theory (DFT) calculations were performed using the projector-augmented wave (PAW) method and the Perdew-Burke-Ernzerhof generalized gradient approximation (PBE-GGA) exchange correlation functional.[2] The plane wave cutoff was set to 450 eV with a Hellmann-Feynman forces convergence criterion set to be lower than 0.01 eV $Å^{-1}$ during the geometrical optimization. The energy was optimized until the difference between two steps less than 10^{-5} eV. Both structures are separately optimized before combination. The van der Waals interaction was considered by adopting the dispersion correction by virtue of DFT-D2 approach. The vacuum space of 20 Å at least was selected to avoid the interactions between images. The Brillouin zone was sampled using 2×2×1 k-meshes for the optimization of atomic structures. Meanwhile, spin-polarized calculations were performed. To analyze interactions between Li and Mn_3O_4-MXene, MnO-MXene or MXene, the adsorption energies have been estimated by the following equation:

$$E_a = E_{s+Li} - E_s - E_{Li}$$

Where E_a is the adsorption energy, E_{s+Li} stands for the total adsorption energy of structure, E_s is the total energy of Mn_3O_4-MXene, MnO-MXene or MXene, and E_{Li} represents the total energy of Li.

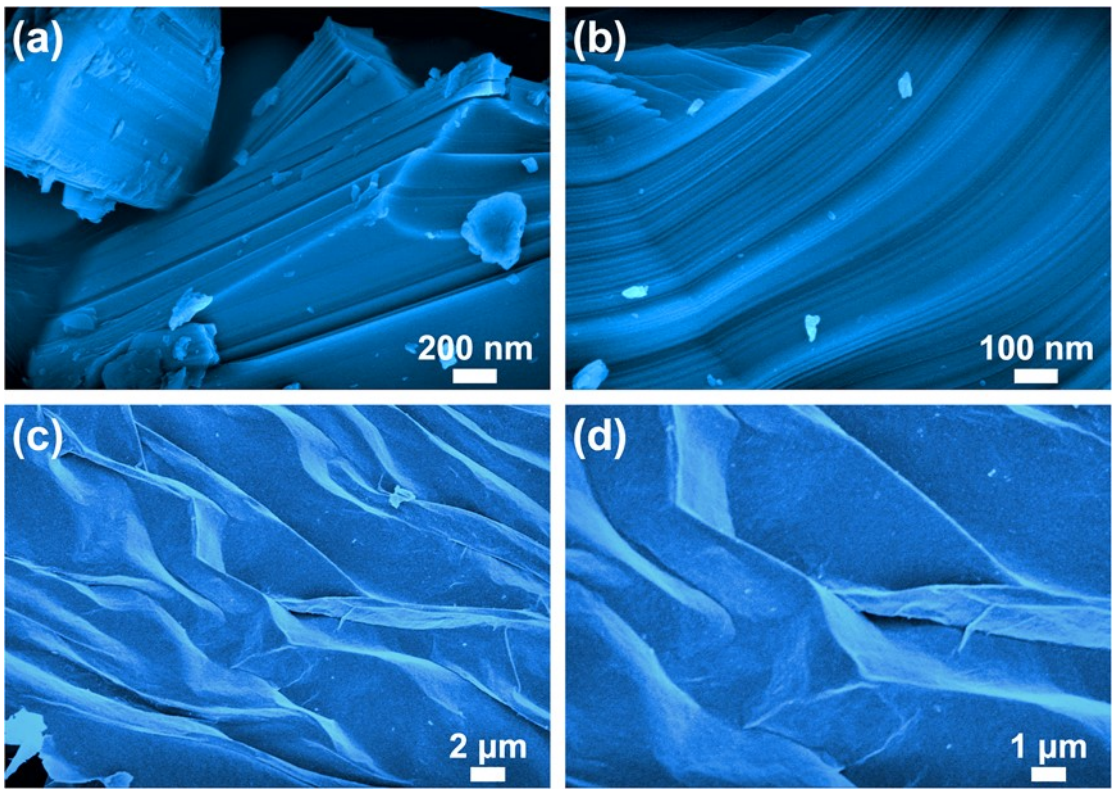

Figure S1. SEM images of Ti_3AlC_2 powders (a, b), and MXene flake (c, d).

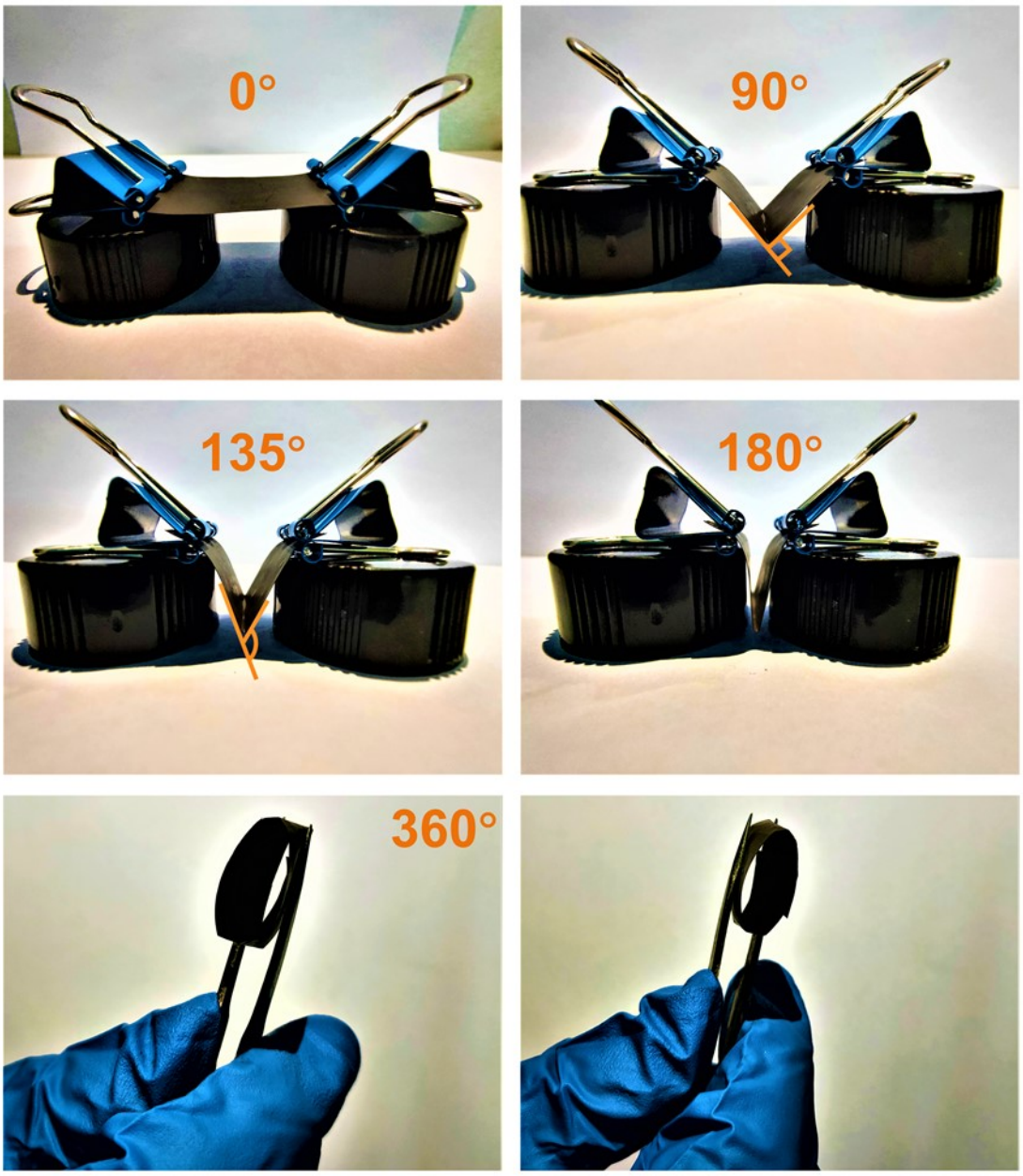

Figure S2. Images of the flexible MnOx-MXene/CNFs membrane during folding and rolling tests from 0º to 360º.

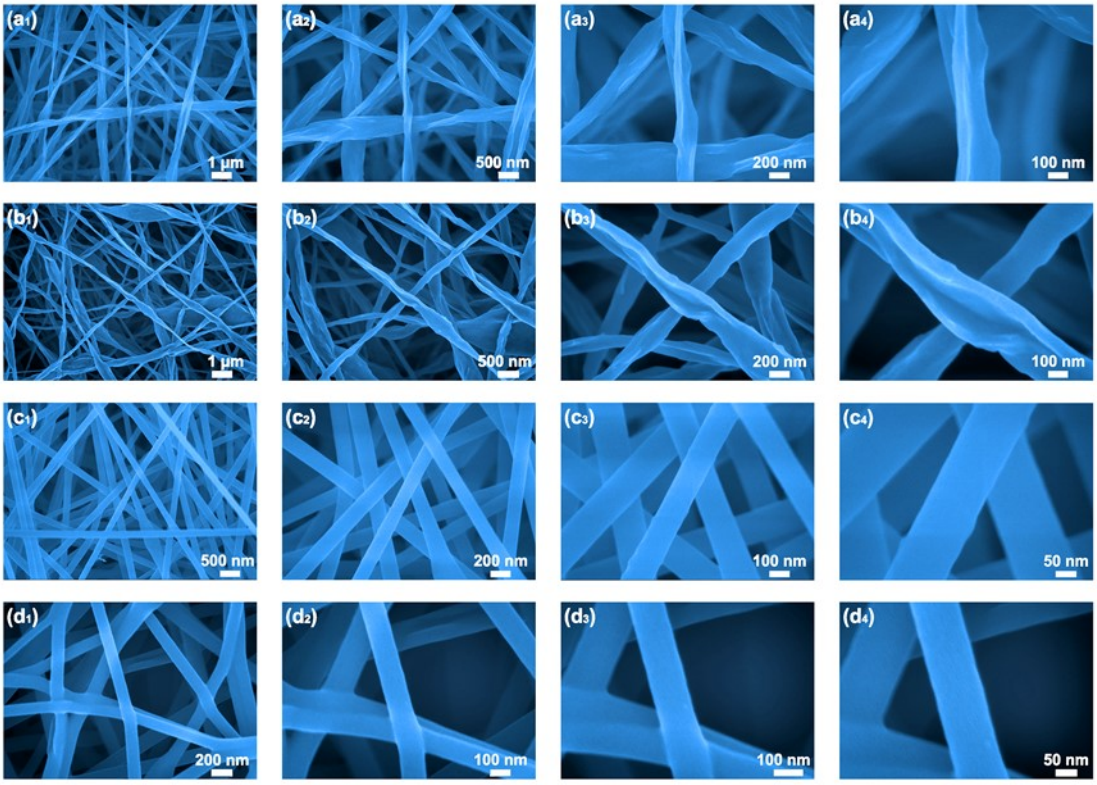

Figure S3. SEM image of MXene/PAN nanofibers ($a_{1\text{-}4}$), MXene/CNFs ($b_{1\text{-}4}$), $Mn(Ac)_2$/PAN nanofibers ($c_{1\text{-}4}$), and MnO_x/CNFs ($d_{1\text{-}4}$).

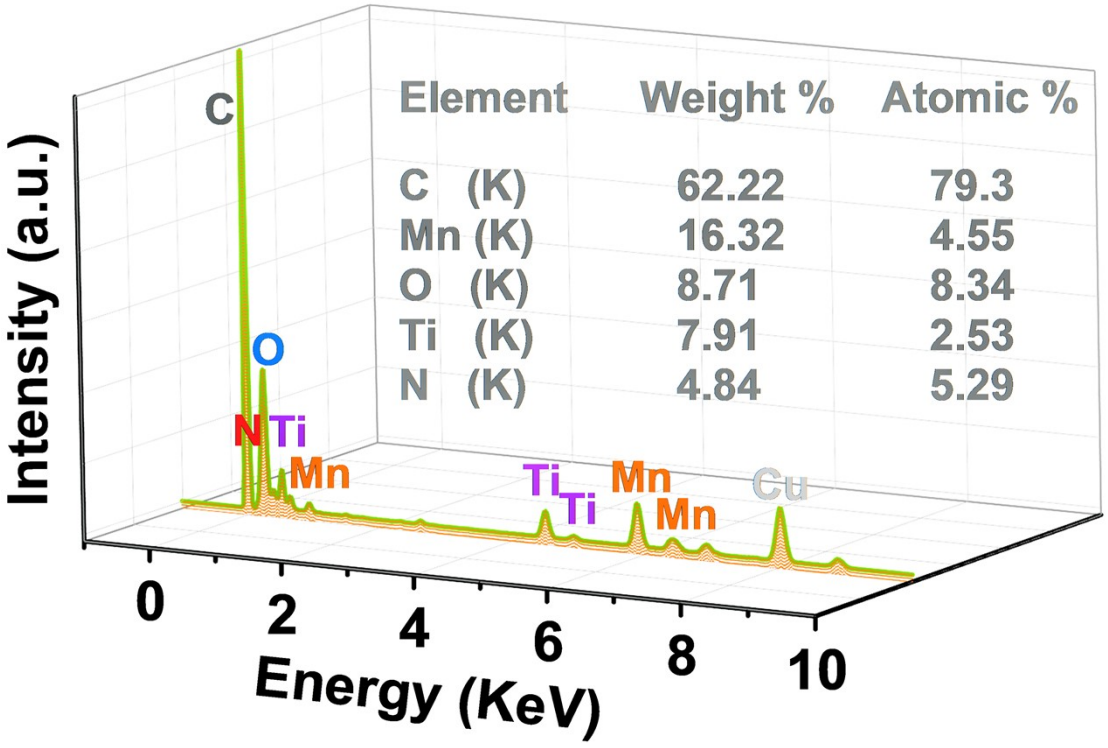

Figure S4. EDS spectrum of MnO_x-MXene/CNFs, where the Cu signals comes from the sample holder.

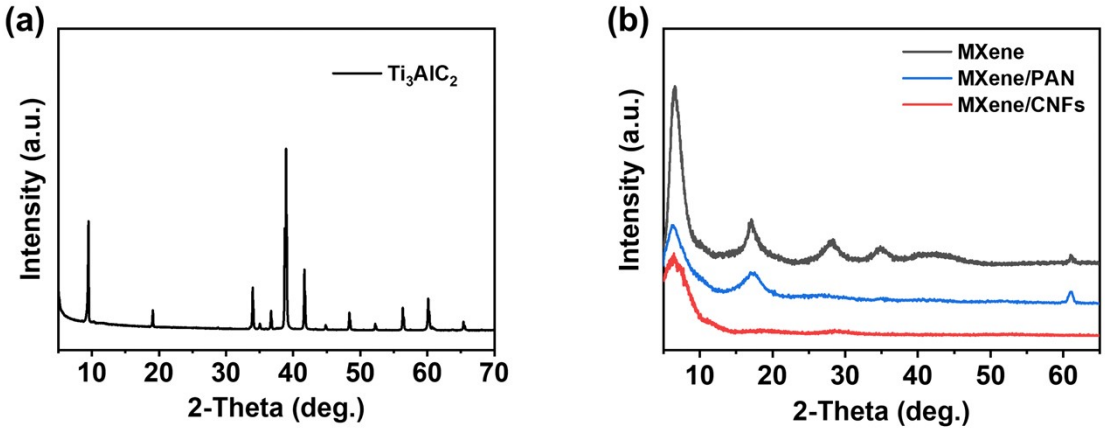

Figure S5. (a)XRD patterns of Ti_3AlC_2 powders; (b)Ti_3C_2 MXene, MXene/PAN nanofibers, and MXene/CNFs.

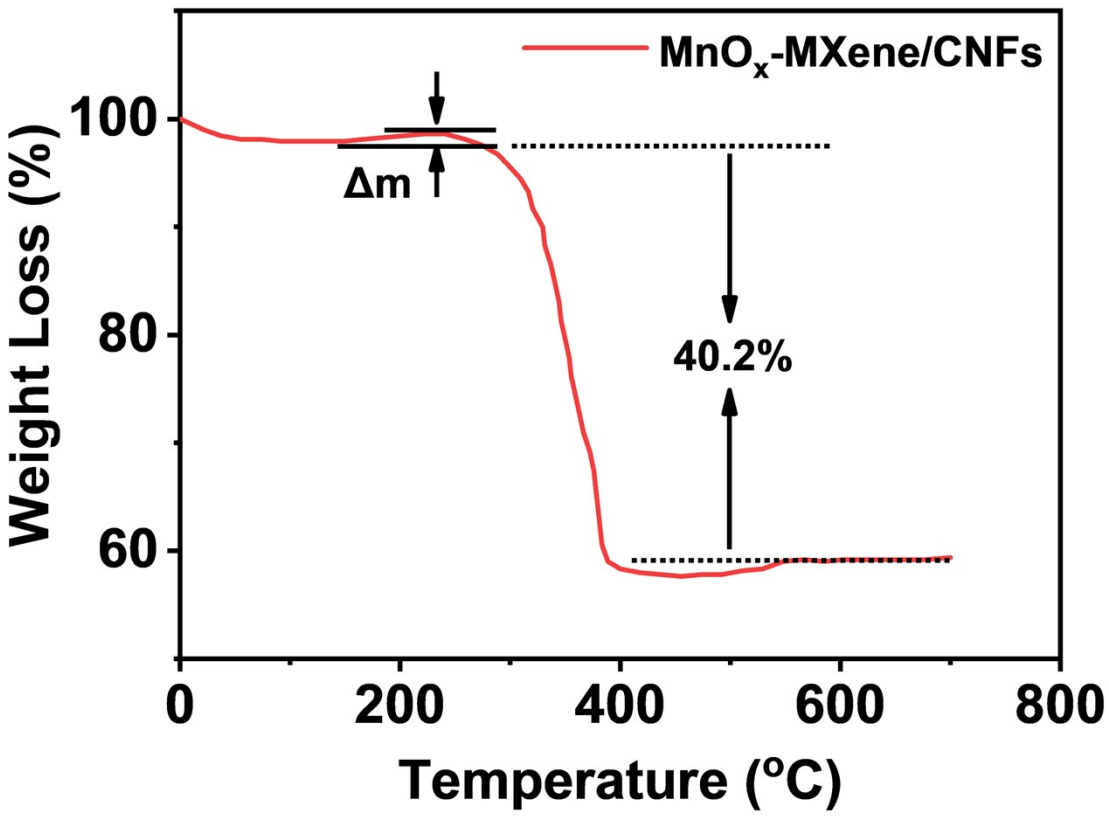

Figure S6. TGA curves of MnO_x-MXene/CNFs.

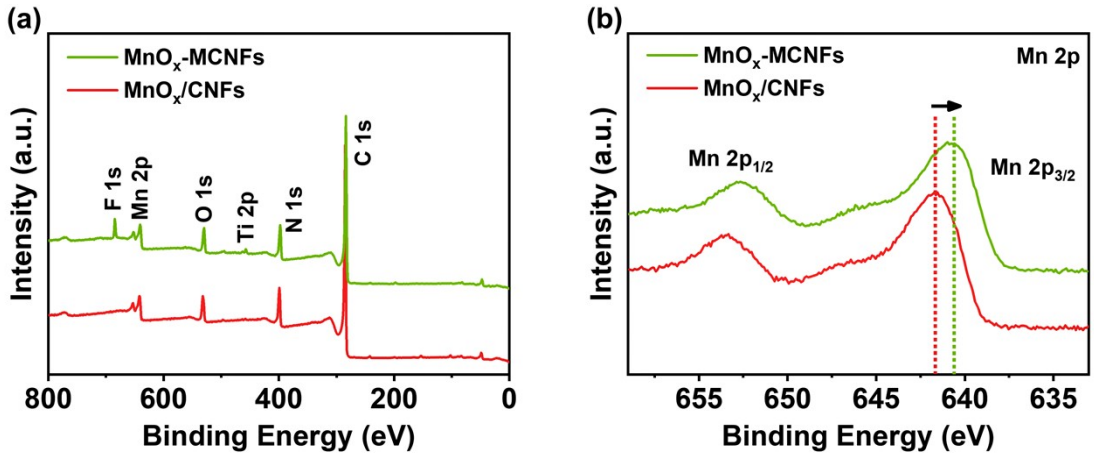

Figure S7. The comparison of XPS survey spectra (a) and high-resolution Mn 2p spectra (b) between MnO_x-Mxene/CNFs and MnO_x/CNFs.

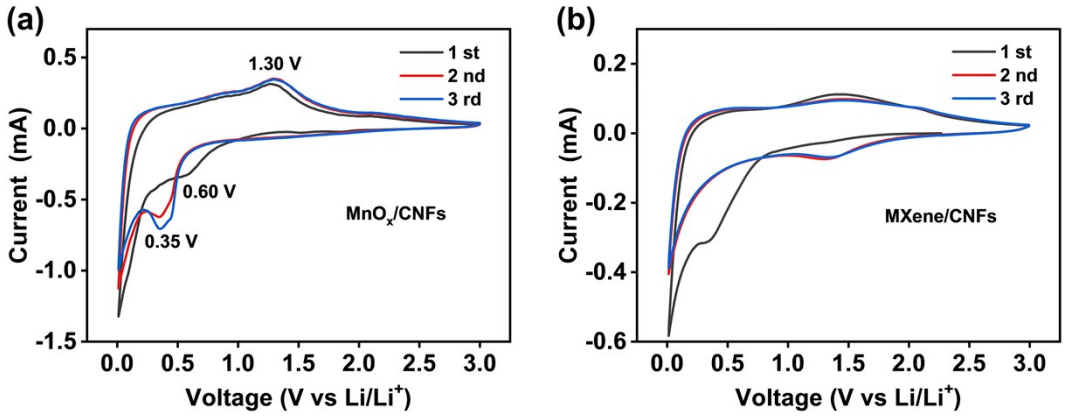

Figure S8. Cyclic voltammograms for the initial three cycles of the (a) MnO_x/CNFs and (b) MXene/CNFs electrodes at a scanning rate of 0.1 mV s^{-1};

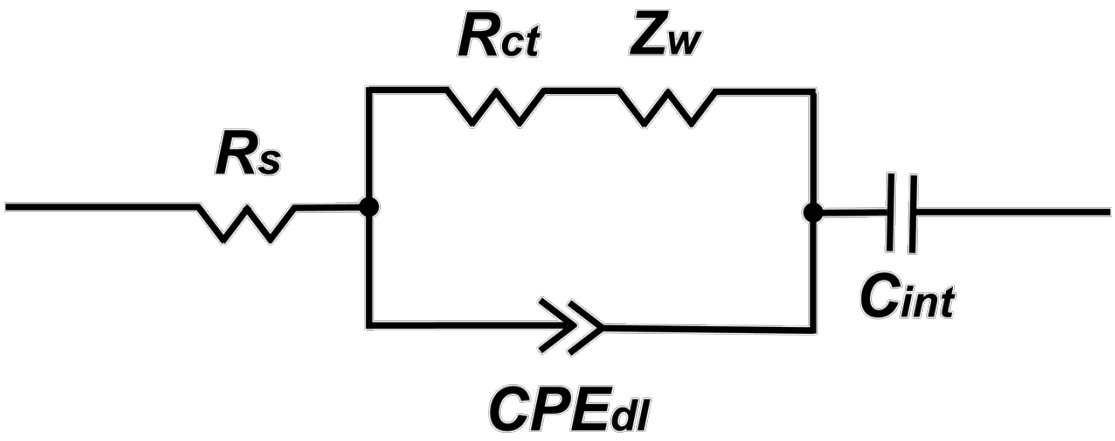

Figure S9. The fitted equivalent circuit model. The constant phase element (CPE) is used to characterize the nature of non-homogeneous for the composite electrode. The circuit elements are R_s (the intrinsic resistance of batteries), R_{ct}//CPE_{dl} (charge-transfer resistance and the double layer (*dl*) capacitance), Z_w (Warburg impedance) and C_{int} is the intercalation capacitance (Li-ion accumulates into particles).

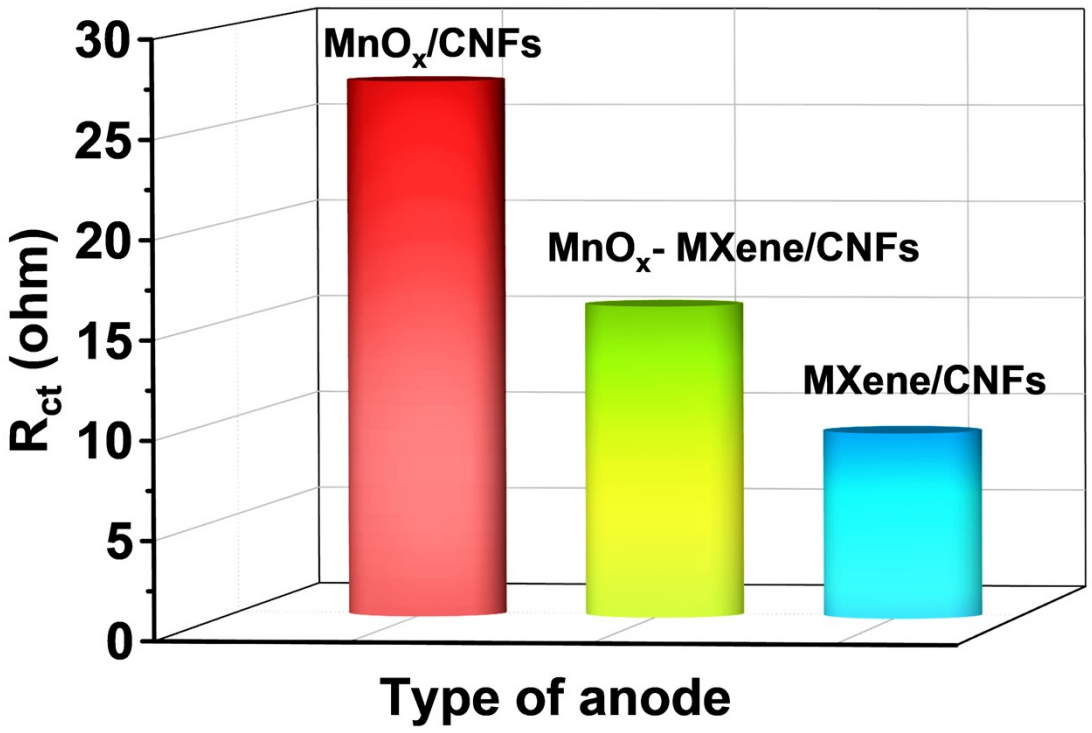

Figure S10. The R_{ct} of MXene/CNFs, MnO_x/CNFs, and MnO_x-MXene/CNFs electrodes.

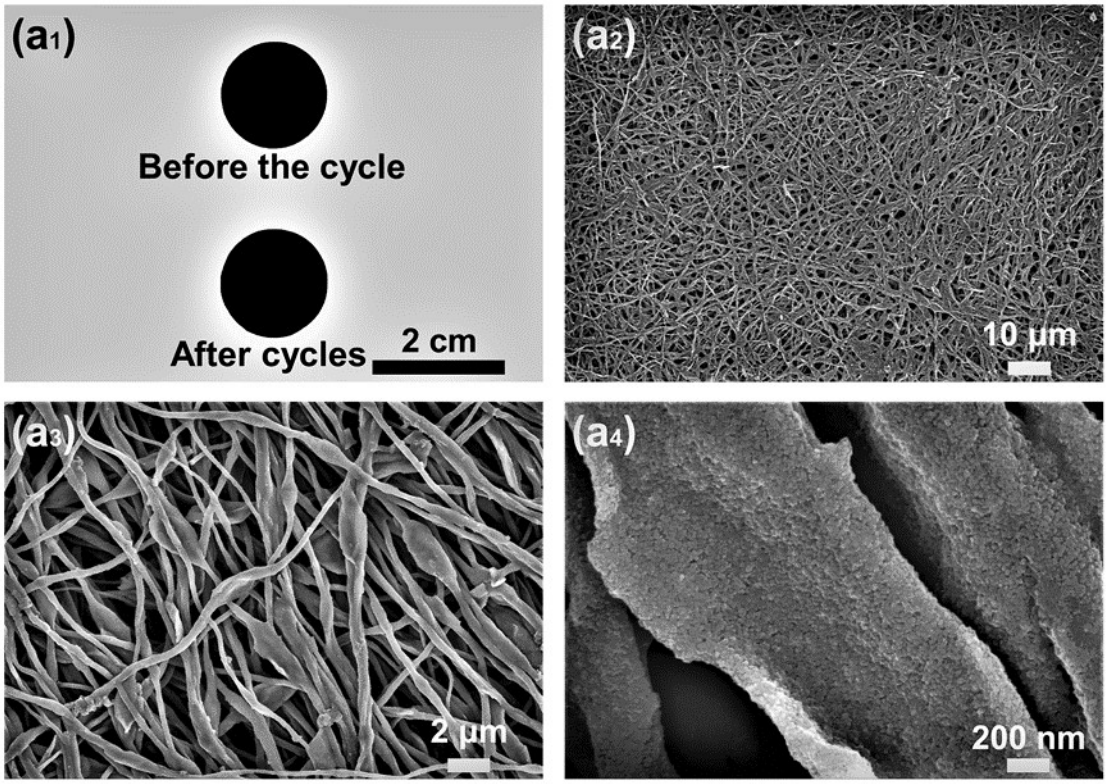

Figure S11. Digital photograph (a_1) and SEM image (a_{2-4}) of MnO_x-MXene/CNFs electrodes after 2000 cycles.

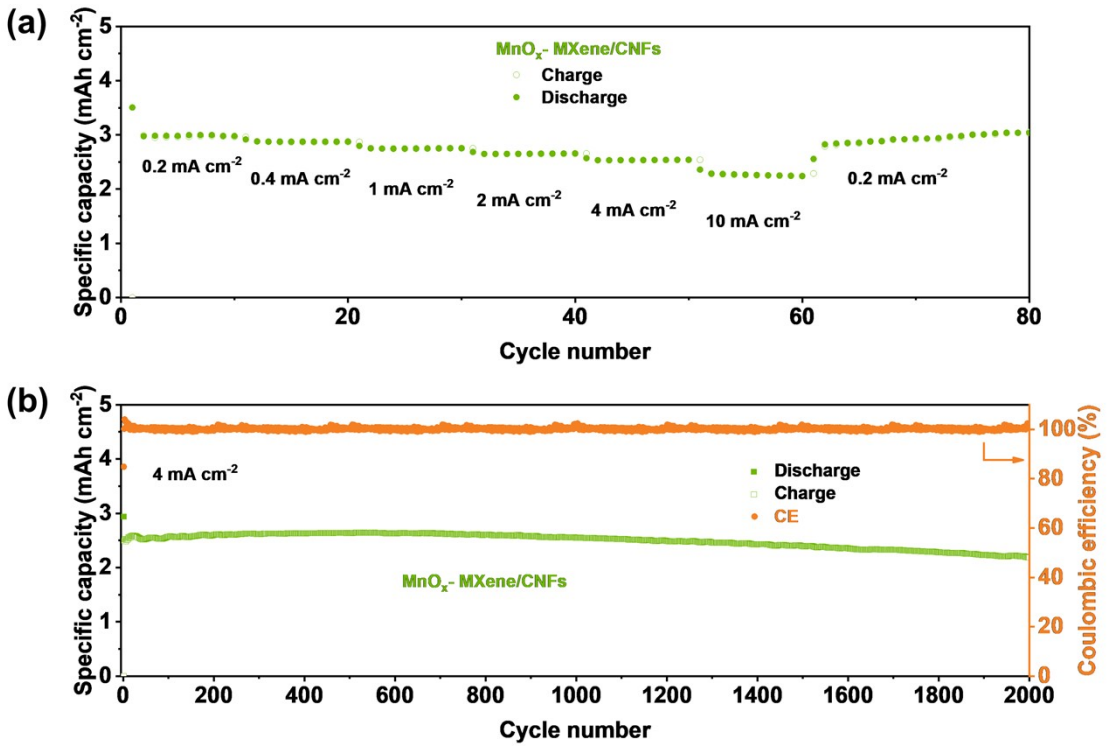

Figure S12. (a) The area specific capacities of the MnO_x-MXene/CNFs anode at different rates (0.2-10 mA cm^{-2}); (b) The long cycling performance of self-supported MnO_x-MXene/CNFs at 4 mA cm^{-2}.

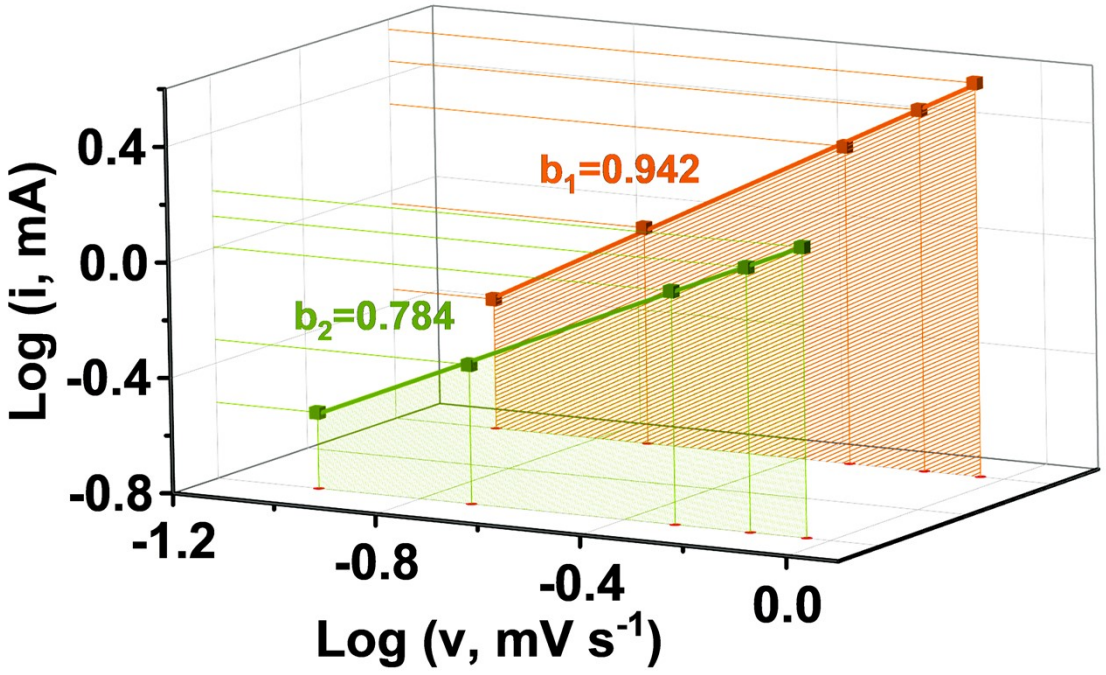

Figure S13. Linear relationship between log (peak current) versus log (scan rate) of MnOx-MXene/CNFs electrode.

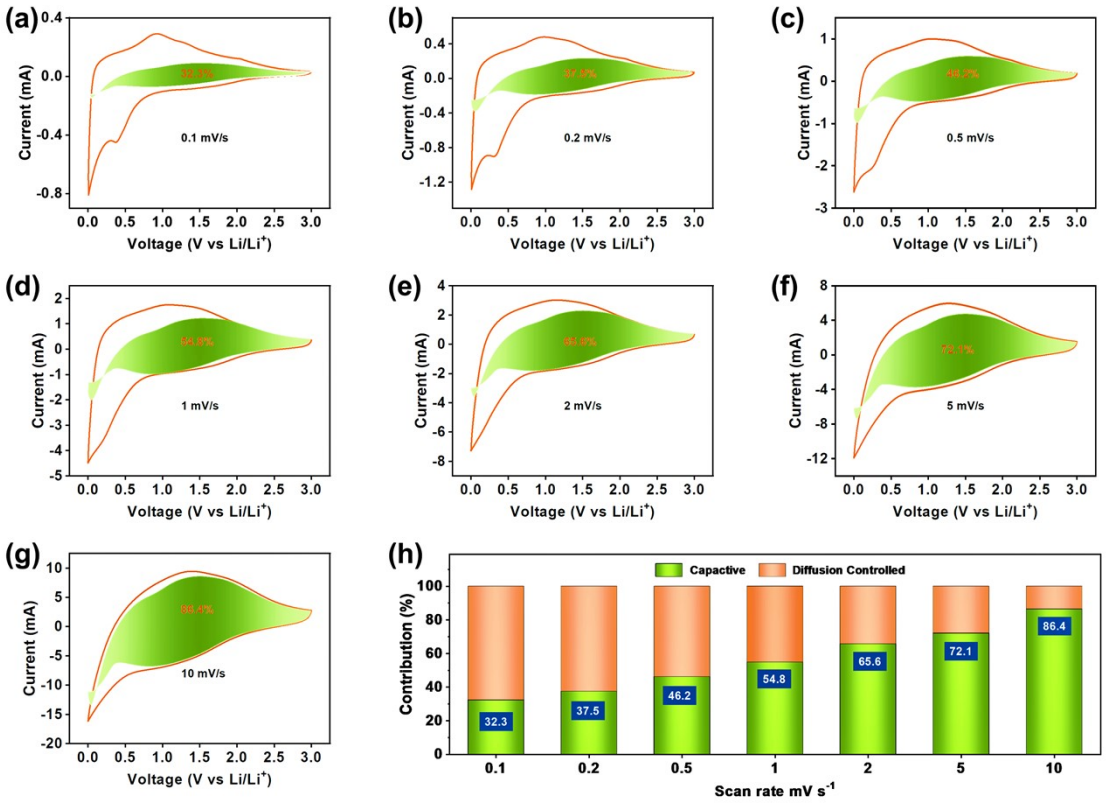

Figure S14. (a-g) The pseudocapacitive contributions of MnOx-MXene/CNFs electrode at different scanning rates from 0.1 mV s^{-1} to 10 mV s^{-1}; (h) Pseudocapacitive contributions at the different scanning rates.

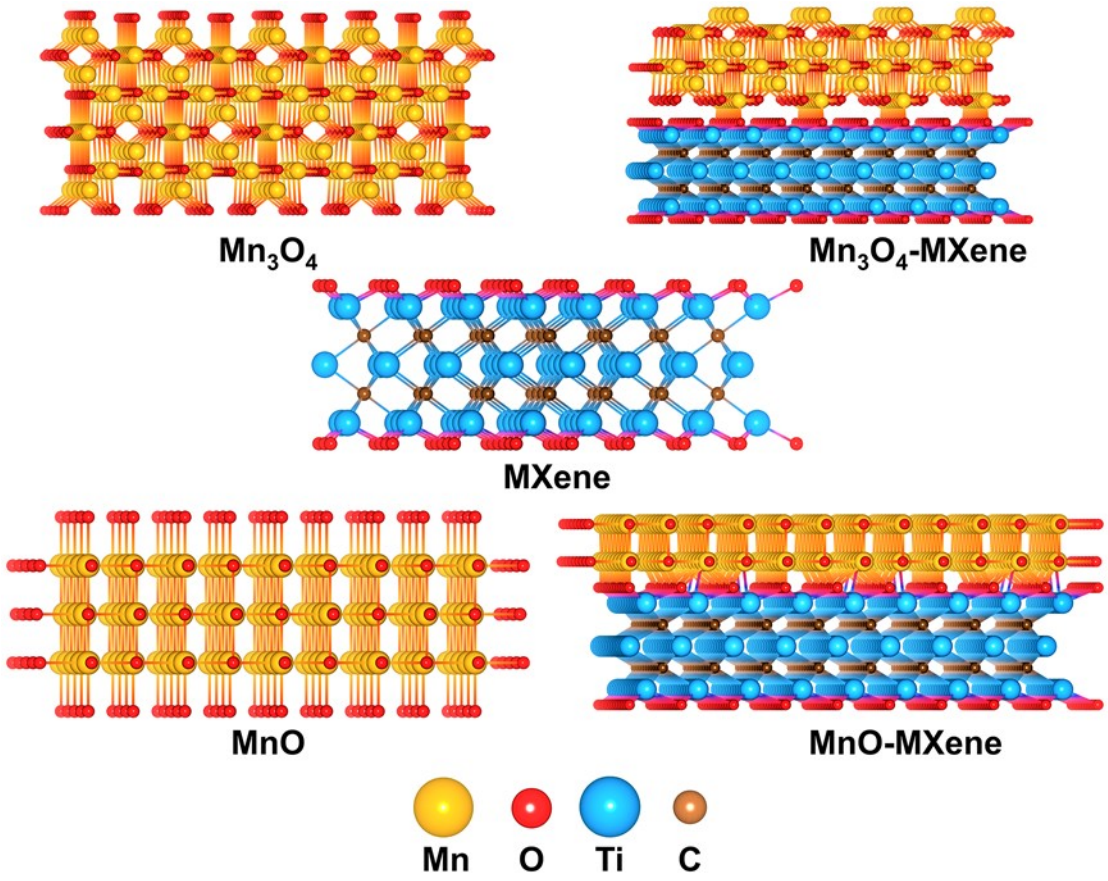

Figure S15. Crystal structures of Mn_3O_4, MnO, MXene, Mn_3O_4-MXene, and MnO-MXene.

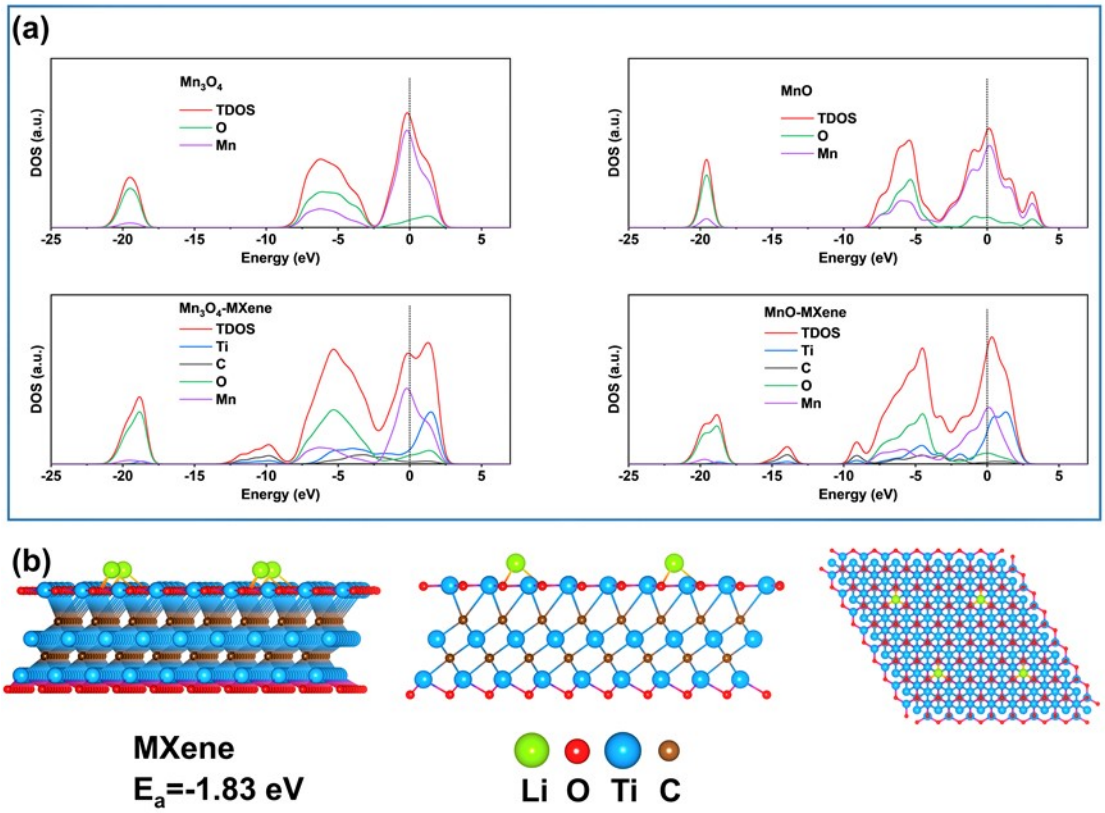

Figure S16. (a) The calculated total density of states (TDOS) and partial density of states (PDOS) of Mn_3O_4, MnO, Mn_3O_4-MXene, and MnO-MXene; (b) The lithium adsorption configuration of MXene.

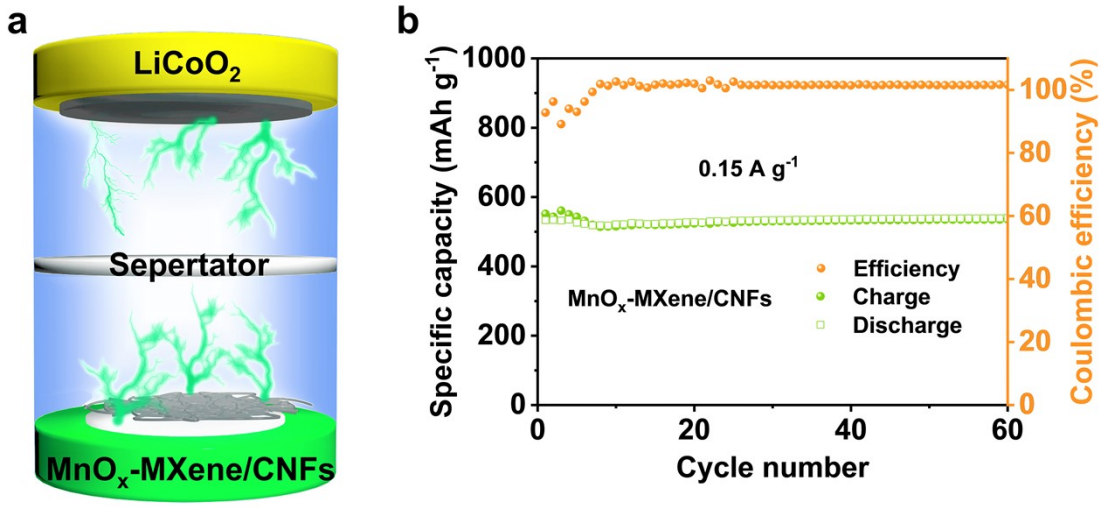

Figure S17. (a)Schematic diagram of the full-cell with the cathodic $LiCoO_2$ and anodic MnO_x-MXene/CNFs; (b) Cycling stability of the full-cell at 0.15 A g^{-1}.

Table S1. Initial discharge capacities and initial coulombic efficiency (CE) of MnO_x-MXene/CNFs, MnO_x/CNFs, and MXene/CNFs at 2 A g^{-1}.

Sample	Initial discharge capacity (mAh g^{-1})	Initial coulombic efficiency (%)
MnO_x-MXene/CNFs	**1468.47**	**84.85**
MnO_x/CNFs	1338.88	69.75
MXene/CNFs	273.68	60.88

Table S2. Fitted impedance parameters and equivalent circuit.

Sample	R_s (Ω)	R_{ct} (Ω)
MnO_x-MXene/CNFs	**1.430**	**15.899**
MnO_x/CNFs	5.460	27.199
MXene/CNFs	1.557	9.352

Table S3. Li ion adsorption ability of Mn_3O_4-MXene, MnO-MXene, and MXene.

Sample	E_a (eV)	E_{S+Li} (eV)	E_S (eV)	E_{Li} (eV)
Mn_3O_4-MXene	**-2.1855**	-403.33564	-400.91835	-0.2318
MnO-MXene	**-2.1637**	-180.49049	-178.09499	-0.2318
MXene	-1.8322	-250.748	-248.684	-0.2318

Table S4. Capacity retention of the MnO_x-MXene/CNFs anode obtained in this work compared with various MnO_x-based anode materials as reported in the literature.

Anode materials	Current density (A g^{-1})	Cycle number	Specific capacity (mAh g^{-1})	Reference
MnO_x-MXene/CNFs	2	2000	1098	**This work**
Yolk–shell MnO_x@NC	2	1000	400	[3]
PSCMnO_x@G	2	500	1162	[4]
CNF/MnO	0.2	100	824	[5]
Mn_3O_4@NC	1	1000	960	[6]
C/MnO_x/CNT	0.5	500	600	[7]
b-MnO_2 ALAT	1	2500	520	[8]
MnO_x/MWCNTs	2	1000	700	[9]

References

1. Y. Guo, D. Zhang, Y. Yang, Y. Wang, Z. Bai, P. K. Chu and Y. Luo, *Nanoscale*, 2021, **13**, 4624-4633.
2. W. Yang, J. Zhou, S. Wang, W. Zhang, Z. Wang, F. Lv, K. Wang, Q. Sun and S. Guo, *Energy Environ. Sci.*, 2019, **12**, 1605-1612.
3. C. Yang, Y. Yao, Y. Lian, Y. Chen, R. Shah, X. Zhao, M. Chen, Y. Peng and Z. Deng, *Small*, 2019, **15**, 1900015.
4. C. Xu, Z. Liu, T. Wei, L. Sheng, L. Zhang, L. Chen, Q. Zhou, Z. Jiang, L. Wang and Z. Fan, *J. Mater. Chem. A*, 2018, **6**, 24756-24766.
5. T. Wang, H. Li, S. Shi, T. Liu, G. Yang, Y. Chao and F. Yin, *Small*, 2017, **13**, 1604182.
6. Y. Qin, Z. Jiang, L. Guo, J. Huang and Z.-J. Jiang, *Chem. Eng. J.*, 2021, **406**, 126894.
7. H. Liu, J.-G. Wang, W. Hua, J. Wang, D. Nan and C. Wei, *Chem. Eng. J.*, 2018, **354**, 220-227.
8. B. Jia, W. Chen, J. Luo, Z. Yang, L. Li and L. Guo, *Adv. Mater.*, 2020, **32**, 1906582.
9. X. Guo, Z. Sun, H. Ge, Q. Zhao, T. Shang, Y. Tian and X.-M. Song, *Chem. Eng. J.*, 2021, **426**, 131335.